

Predicting Hurricane Intensity and Structure Changes Associated with Eyewall Replacement Cycles

JAMES P. KOSSIN

NOAA/National Climatic Data Center, Asheville, North Carolina, and Cooperative Institute for Meteorological Satellite Studies, Madison, Wisconsin

MATTHEW SITKOWSKI

Cooperative Institute for Meteorological Satellite Studies, and Department of Atmospheric and Oceanic Sciences, University of Wisconsin—Madison, Madison, Wisconsin

(Manuscript received 25 September 2011, in final form 2 December 2011)

ABSTRACT

Eyewall replacement cycles are commonly observed in tropical cyclones and are well known to cause fluctuations in intensity and wind structure. These fluctuations are often large and rapid and pose a significant additional challenge to intensity forecasting, yet there is presently no objective operational guidance available to forecasters that targets, quantifies, and predicts these fluctuations. Here the authors introduce new statistical models that are based on a recently documented climatology of intensity and structure changes associated with eyewall replacement cycles in Atlantic Ocean hurricanes. The model input comprises environmental features and satellite-derived features that contain information on storm cloud structure. The models predict the amplitude and timing of the intensity fluctuations, as well as the fluctuations of the wind structure, and can provide real-time operational objective guidance to forecasters.

1. Introduction

Typically, the formation of a secondary (outer) concentric eyewall in a hurricane signals an impending fluctuation in the storm's ongoing intensity evolution (Fig. 1). These fluctuations are anomalous in that they constitute a transient behavior that is generally not captured well by the present suite of operational intensity forecast guidance. Consequently, when the formation of a secondary eyewall is observed (or predicted; e.g., Kossin and Sitkowski 2009) in an operational setting, forecasters must rely on expert judgment that is based on experience to subjectively modify the intensity forecasts provided by the available objective guidance.

Recently Sitkowski et al. (2011, hereinafter SKR11) used low-level aircraft reconnaissance data to construct an expanded climatology of intensity and structure changes associated with eyewall replacement cycles (ERC) in Atlantic Ocean hurricanes. Aircraft data were found to capture the amplitude of the transient

fluctuations better than best-track data, primarily because the best track provides a temporally smoothed evolution. A caveat to using aircraft data is that the data are limited in their spatial sampling and are not necessarily representative of the maximum intensity as provided by best-track data. Another caveat to using aircraft data is that they are generally sporadic in time and do not typically capture the full evolution of an ERC. However, SKR11 were able to identify and document 24 complete ERCs in their expanded aircraft dataset and found that a typical ERC can be naturally divided into three distinct phases (Fig. 1). The average intensity and structure changes associated with those phases are summarized here in Table 1.

In this work, we exploit the characteristics of these changes to construct empirical/statistical models that can provide objective real-time guidance to forecasters. The models predict the expected intensity changes and the duration over which these changes occur during the most operationally relevant phases of an ERC. Additionally, the models provide predictions of expected radial changes in tangential wind structure, which may be useful for wave-height and storm-surge forecasting.

Corresponding author address: James Kossin, CIMSS, University of Wisconsin—Madison, 1225 W. Dayton St., Madison, WI 53706.
E-mail: james.kossin@noaa.gov

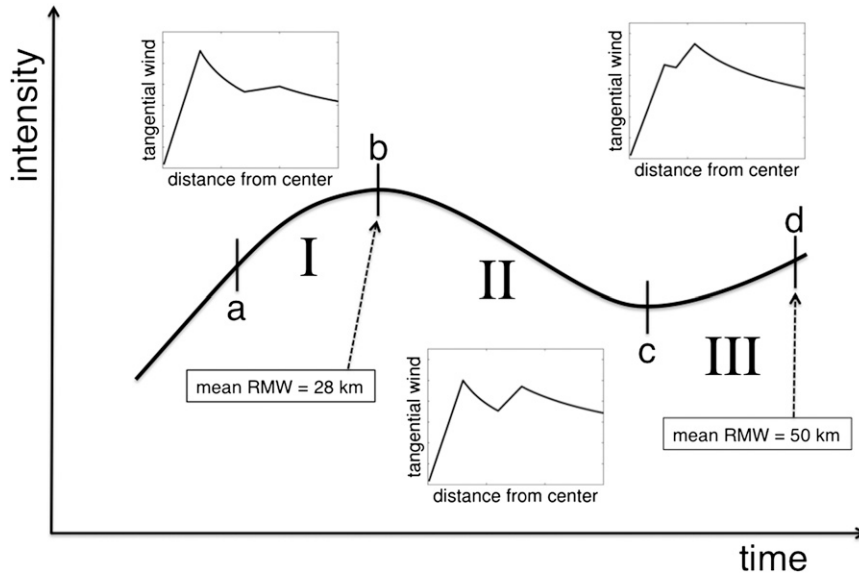


FIG. 1. Mean evolution of a hurricane eyewall replacement cycle (ERC). Here the beginning of the ERC (point a) is identified by a persistent coherent secondary wind maximum observed at flight level. This marks the beginning of the intensification phase (I) of the ERC. During this phase, both the primary (inner) and secondary (outer) wind maxima are increasing and contracting. During the weakening phase (II), the primary wind maximum decreases while the secondary maximum increases as it contracts inward. The end of the weakening phase (point c) is identified when both wind maxima are equal. Beyond point c, the outer wind maximum has exceeded the inner one and is now the primary maximum. During the reintensification phase (III), the outer wind maximum continues to contract inward while intensifying. The three inset figures represent typical radial profiles of flight-level tangential wind observed during the three phases. The ERC is completed (point d) when there is no longer an observed inner wind (local) maximum. At this time, the mean intensification rate is about one-half of that observed at the start of the ERC (at point a). The mean radius of maximum wind at points b and d is 28 and 50 km, respectively.

2. Methods

In SKR11, all flight-level wind profiles available for the 24 complete ERC cases were fit to a parametric profile with a number of adjustable parameters. Here, we will concentrate on four of these parameters: the inner and outer wind maxima and their radii (Fig. 2). In

particular, we are interested in how these four parameters change during an ERC. It is generally within phase I that forecasters begin to increase their focus on indicators that an ERC may be imminent. These indicators would typically include the presence of coherent secondary wind maxima observed by low-level aircraft reconnaissance or an apparent tendency toward axisymmetric

TABLE 1. Mean changes in the intensity and radial structure parameters v_1 , v_2 , r_1 , and r_2 (as shown in Fig. 2) during each of the three ERC phases, and the mean duration Δt of each phase. Also shown are the associated standard deviations (SD). All values are based on the 24 ERC events described in the text. For comparison, changes in best-track intensities $\Delta v_{\text{best-track}}$ interpolated to the periods of the phases are also shown, and demonstrate how the smoothed nature of the best track significantly underestimates the fluctuations associated with ERCs (this table is adapted from SKR11).

	Intensification		Weakening		Reintensification		
	Mean	SD	Mean	SD	Mean	SD	
Δv_1 (kt)	+14	18	-20	11	-15	14	Mean total change in max flight-level intensity = +2 kt
Δv_2 (kt)	+9	11	+18	14	+8	8	
$\Delta v_{\text{best-track}}$ (kt)	+7	11	-9	12	-2	5	
Δr_1 (km)	-7.0	11.5	-1.4	6.9	-2.2	8.0	Mean total duration = 36.7 h
Δr_2 (km)	-14.8	18.8	-28.8	15.9	-12.7	12.0	
Δt (h)	9.4	9.1	16.6	8.6	10.7	12.6	

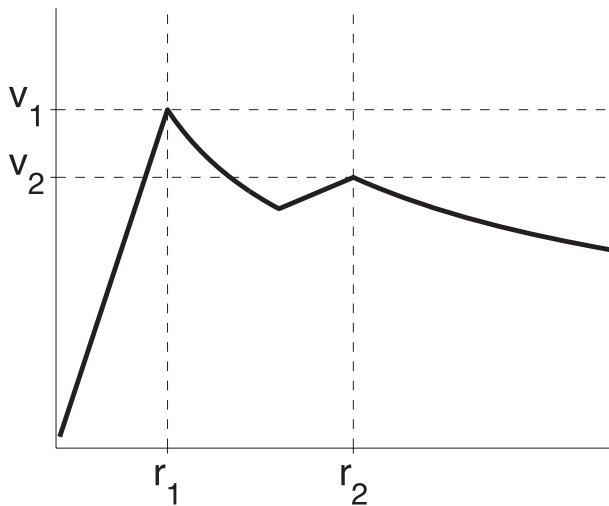


FIG. 2. Generic tangential wind profile with inner (v_1) and outer (v_2) maxima at radii r_1 and r_2 , respectively. The characteristic changes of v_1 , v_2 , r_1 , and r_2 during an ERC are shown in Table 1.

organization of convective rainbands in satellite microwave or land/aircraft-based radar imagery. In addition to these indicators, objective guidance that provides probability of ERC initiation has recently been made operationally available (Kossin and Sitkowski 2009).

In a typical forecasting scenario then, with an intensity forecast being made during phase I of an ERC, a practical question would be “How much weakening is expected and when will the storm begin to reintensify?” In terms of our parameters, this translates to “How much is inner tangential wind maximum v_1 expected to decrease during phase II of the ERC and what is the expected duration of phase II?” Similarly, the question “At what rate will the storm reintensify after the weakening period?” requires predicting the rate of increase of outer tangential wind maximum v_2 during phase III (note that v_2 is greater than v_1 during phase III and represents the storm’s maximum intensity in this period).

As demonstrated by SKR11, each phase of an ERC has a characteristic duration and intensity change associated with it (Table 1). For example, the mean duration of the weakening phase is 16.6 h and the mean intensity change is -20 kt ($1 \text{ kt} \approx 0.5 \text{ m s}^{-1}$), whereas the reintensification phase typically spans 10.7 h with a mean intensity change of $+8$ kt. However, as also shown by the standard deviations in Table 1, the variance associated with these values can be large. Our goal is to construct models that explain part of this variance using operationally available information.

The models constructed here are based on standard stepwise linear regression with forward selection (Wilks 2006), and the predictors are taken from the operational

predictor suite of the Statistical Hurricane Intensity Prediction Scheme (SHIPS; DeMaria et al. 2005). As described above, the models are designed to provide information under the assumption that a hurricane has entered phase I of an ERC and is approaching the onset of phase II (point b in Fig. 1). Except for the satellite-based features, the predictors used to train and test the models represent the conditions integrated from point b in Fig. 1 to 24 h into the future (i.e., they represent an average of current conditions derived from analyses and predicted conditions derived from model prognostic fields). All of these diagnostic and prognostic values are readily available in the SHIPS predictor suite. The SHIPS satellite-based features measured at point b are also used (these features are not predicted by models and are only diagnostic predictors).

The forward selection is performed with the usual requirement that the coefficients of the predictors be significant at the 95% level or greater. After the forward selection, each model is tested for robustness with a leave-one-out procedure in which each of the 24 ERC events is removed from the sample and the model is reconstructed with the remaining 23 events. If any regression coefficient in any one of the resulting models is not significant at the 95% level or greater, that predictor is discarded and the process is repeated with the remaining predictors. This procedure also provides a cross validation (i.e., independent testing) from which the root-mean-square (RMS) error is derived for the final models.

To provide intensity forecasting guidance during an ERC, three models are constructed to predict 1) Δv_1 during phase II, 2) Δt of phase II, and 3) the rate of change of v_2 during phase III. The predictand of the second model (Δt) should always be positive and is logarithmically transformed in the regression. To provide forecast guidance on wind structure changes, a fourth model is constructed to predict the total change in radius of maximum wind (RMW) during phases II and III.

It should be emphasized that the models predict intensity and structure fluctuations along or near the 700-hPa flight level and not at the surface, which is more relevant to actual forecast metrics. Since corrections from flight level to the surface are generally performed with constant multiplicative factors at any fixed radius from the storm center and we are only considering changes and not absolute values, the values predicted by the models are expected to reasonably represent changes at the surface. Still, it should be recognized that changes associated with ERCs may behave in unique ways and that any height-dependent changes that occur will introduce some additional error in the model predictions. It is beyond the scope of this paper to explore

TABLE 2. SHIPS predictors chosen in the stepwise regressions. Here, GOES is Geostationary Operational Environmental Satellite.

Predictor	Description
VMX	Current intensity (kt)
LAT	Lat ($^{\circ}$)
SHRD	Avg 850–200-hPa shear magnitude (kt) in the annulus $r = 200$ –800 km
VMPI	Max potential intensity (kt) as calculated following Bister and Emanuel (1998)
TWAC	Avg 850-hPa symmetric tangential wind (m s^{-1}) in the annulus $r = 0$ –600 km
IR00_02	Avg GOES channel-4 brightness temperature ($^{\circ}\text{C}$) in the annulus $r = 0$ –200 km
IR00_17	Radius (km) of min GOES brightness temperature within $r = 20$ –120 km

this, but is offered here as an interesting question that might be addressed in the future with the inclusion of surface data from airborne microwave radiometers or dropsondes.

As noted in Fig. 1, the end of phase III (as defined by SKR11) is realized when there is no longer an observed inner wind (local) maximum. At this time, the mean intensification rate is about one-half of that observed at the start of the ERC and the mean RMW has expanded by a factor of about 2. There is no obvious physical relevance associated with the moment that the local inner wind maximum is no longer observable, and phase III just marks the period when the models introduced here become less applicable and the traditional intensity forecast guidance tools, such as SHIPS, may require less adjustment. In this sense, the new models provide a temporary patch to be applied during an ERC, and the predicted rate of change of v_2 during phase III is provided as information during the period of relinquishing control to the more standard guidance models.

3. Results

A description of the four models is summarized in Tables 2 and 3. The amount of weakening during phase

II is related to the current intensity entering the phase, the storm latitude, and the environmental vertical wind shear. Storms that are stronger, or that are located at higher latitudes, or that are embedded in higher shear tend to weaken more during an ERC. The duration of the weakening phase is related to the satellite infrared brightness temperature at the onset of the phase. In particular, the duration is longer when the coldest cloud tops are located farther away from the storm center. The reintensification rate during phase III is related to environmental potential intensity (PI; designated as VMPI in Table 2) and the satellite brightness temperature, with lower PI and colder cloud tops associated with faster rates. The relationship with PI appears to be somewhat counterintuitive, but a possible explanation may be deduced from the fourth model in Table 3. The expansion of the RMW across the weakening and reintensification phases is also related to PI, with higher PI associated with greater expansion. That is, ERCs occurring in higher PI tend to result in storms with larger eyes. These storms are observed to maintain a more constant intensity (e.g., Knaff et al. 2003), and thus higher PI may control reintensification through its effect on RMW expansion.

4. Concluding remarks

The four models introduced here exhibit apparently useful predictability of the predictands, and the amount of variance explained ranges from 47% to 68%. RMS errors calculated through leave-one-out cross validation (i.e., independent testing) suggest that the models can improve skill in an operational setting. The small size of the sample ($N = 24$) used to construct and test the models, however, prescribes some caution regarding expectations, particularly in a real-time environment where predictors may take on values outside of their range in the training sample. Still, the models can provide the first objective forecast guidance for predicting anomalous intensity and wind structure changes associated with ERCs, and are expected to improve over time as the

TABLE 3. Description of the models, including the variance explained R^2 , the p value of the regression, and the RMS error from leave-one-out cross validation.

Predictand	Model	R^2 , p value, and RMS error
Δv_1 in phase II (kt) (amount of weakening)	$\Delta v_1 \approx 81.16 - 0.523\,171 \times \text{VMX} - 1.294\,89 \times \text{LAT} - 0.757\,874 \times \text{SHRD}$	0.68, 0.000 09, 3.6 kt
Δt in phase II (h) (duration of weakening)	$\Delta t \approx \exp(1.742\,37 + 0.015\,696\,4 \times \text{IR00_17})$	0.49, 0.0004, 6.2 h
dv_2/dt in phase III (kt h^{-1}) (rate of reintensification)	$dv_2/dt \approx 2.228\,18 - 0.102\,873 \times \text{VMPI} - 0.222\,671 \times \text{IR00_02}$	0.47, 0.003, 1.3 kt h^{-1}
ΔRMW (km) (change in RMW from onset of weakening to end of ERC)	$\Delta \text{RMW} \approx -99.3306 + 1.039\,14 \times \text{VMPI} - 1.780\,98 \times \text{TWAC}$	0.51, 0.001, 9.9 km

sample size of the training dataset grows. The models were designed to be applied operationally and offer measurable potential to contribute to reducing short-lead-time intensity forecast errors. The models also provide an easily adaptable platform for further improvements that might be gained with the inclusion of predictors beyond those available through SHIPS, such as satellite microwave-based features.

Acknowledgments. This work is funded by NOAA through the USWRP Joint Hurricane Testbed and the National Climatic Data Center. The authors are grateful to Mark DeMaria and two anonymous reviewers for their comments on the manuscript.

REFERENCES

- Bister, M., and K. A. Emanuel, 1998: Dissipative heating and hurricane intensity. *Meteor. Atmos. Phys.*, **52**, 233–240.
- DeMaria, M., M. Mainelli, L. K. Shay, J. A. Knaff, and J. Kaplan, 2005: Further improvements to the Statistical Hurricane Intensity Prediction Scheme (SHIPS). *Wea. Forecasting*, **20**, 531–543.
- Knaff, J. A., J. P. Kossin, and M. DeMaria, 2003: Annular hurricanes. *Wea. Forecasting*, **18**, 204–223.
- Kossin, J. P., and M. Sitkowski, 2009: An objective model for identifying secondary eyewall formation in hurricanes. *Mon. Wea. Rev.*, **137**, 876–892.
- Sitkowski, M., J. P. Kossin, and C. M. Rozoff, 2011: Intensity and structure changes during hurricane eyewall replacement cycles. *Mon. Wea. Rev.*, **139**, 3829–3847.
- Wilks, D. S., 2006: *Statistical Methods in the Atmospheric Sciences*. 2nd ed. International Geophysics Series, Vol. 91, Academic Press, 627 pp.